A comprehensive hydrodynamic analysis of a full-scale oxidation ditch using Population Balance Modelling in CFD simulation

J. Climent [a], R. Martínez-Cuenca [a], P. Carratalà [a], M.J. González-Ortega [b], M. Abellán [c], G. Monrós [a], S. Chiva[a]*

[a] UNIVERSITAT JAUME I, Department of Mechanical Engineering and Construction. Av. Vicent Sos Baynat, s/n 12071 Castellón (Spain). (E-mail: jcliment@uji.es; raul.martinez@uji.es; pcarrata@uji.es, schiva@uji.es *corresponding author)
[b] Escuela Técnica Superior de Ingeniería Agronómica, Universidad Politécnica de Cartagena. Paseo Alfonso XIII, 48. 30203 Cartagena, Spain. (E-mail: mjgo0@alu.upct.es)
[c] ESAMUR, Entidad de Saneamiento y Depuración de la Región de Murcia, Complejo de Espinardo - Ctra. N-301 C/Santiago Navarro, 4 1ª Planta 30.100 Espinardo (Murcia) (Spain). (E-mail: manuel.abellan@esamur.com)

Abstract: This work exhibits the importance of the experimental validation when full-scale computational fluid dynamics (CFD) models are developed to provide a detailed analysis of the spatial variations in 3D of the fluid flow inside aerated tanks. Single-phase and two-phase CFD models were performed to study the fluid behaviour carefully by means of the velocity profiles and the aeration pattern in a full-scale oxidation ditch. Air hold-up, bubble size distribution and interfacial area density were calculated by polydisperse models where Population Balance Model (PBM) was governed by break-up and coalescence; the free-surface approach allowed the CFD model to describe the three-dimensional effect of bubbly plumes in large scales in detail. Tracer tests were carried out to obtain the flow pattern and the hydraulic distribution of the flow into two wastewater treatment lanes in order to define the boundary conditions for the model correctly. Despite the difficulty of performing velocity measurements of the fluid in 3D, with and without air bubbles, these provided essential information to validate the CFD model. From this analysis, several simulations were performed to improve the hydrodynamics and the operation of the process by relocating the propellers.

Keywords: CFD; Hydrodynamics; Oxidation ditch; Population Balance Model; RTD; Two-phase flow

Highlights

• The CFD model predicted a fluid velocity reduction by 60% when air is supplied.
• The PBM analysis revealed the predominance of the coalescence.
• A very detailed hydraulic validation was carried out by 3D velocity measurements.
• The optimal configuration provided a significant process improvement.

1. Introduction

In recent years, there has been a noticeable increase in the scientific production related to wastewater treatment (WWT) modelling performed with Computational Fluid Dynamics (CFD) techniques. As occurred in other industries, it has evolved into a robust and precise technique for design and optimization of Activated Sludge (AS) systems. Reactors in wastewater treatment plants (WWTP) are typically designed as mixed or as plug flow configurations. However, real reactors often show more complex macroscopic flow structures with negative effects on plant performance and control [1]. A considerable number of CFD studies showed the importance of

[+] schiva@uji.es, Universitat Jaume I, Mechanical Engineering and Construction Department. Av. Vicent Sos Baynat, s/n 12071 Castellón (Spain). Telf: +34 964 728 141

hydrodynamics for the process and modelling of biological reactors [2], the WWT efficiency is influenced not only by the bio-reaction of activated sludge, but also by the fluid behaviour including the bubble/liquid flows. This is the scope of the present study. The CFD techniques may provide a valuable hydrodynamic information of an AS bioreactor in order to apply this understanding to the process [3], especially when the tank has a non-standard design, such as the atypical oxidation ditch configuration studied in this work.

Mixing in oxidation ditch configurations is provided by propellers and aerators, which are either superficial or submerged. The objective of the propellers is maintaining the biomass suspended and provide velocity to the flow across the channels, while aeration which is the oxygen source for the process, also induces mixing energy by creating turbulence in the system [4]. In the case of submerged aeration systems CFD studies, authors have mostly investigated the mixing pattern of the aeration tanks from the point of view of the aeration efficiency, e.g. pointing out the influence of the diffuser layout and the axial liquid velocity on the oxygen mass transfer coefficient [5–8]. Unlike other works in this field, this study aims to obtain a deeper understanding of the CFD liquid-gas approach as well as the experimental validation, to reproduce hydrodynamics more faithfully in 3D to be applied to the aeration process in full-scale biological reactors.

To date, CFD models have been primarily used for evaluation of hydraulic problems in different process units of WWTP in order to optimize the design and operation. Dynamic simulation of a whole WWTP is still not feasible and it would not be cost-effective. Authors agree that one of the major bottlenecks of using CFD is its high

[+] schiva@uji.es, Universitat Jaume I, Mechanical Engineering and Construction Department. Av. Vicent Sos Baynat, s/n 12071 Castellón (Spain). Telf: +34 964 728 141

computational requirement [9]. On the one hand, CFD modelling of full-scale biological reactors defined as a single-phase modelling is the most widespread approach because it takes less calculation time than multiphase fluid models to reproduce suspended solids in liquid systems. Even with non-Newtonian fluid approach [10], good predictions of concentrated solid-liquid systems can be achieved in a reduced computing time [11].

Although the sedimentation of the solids in the mixed-liquor can be taken into account by implementing the drift-flux model [12] provided that the minimum velocity of the mixed liquor to keep the solids suspended is ensured [13], single-phase CFD models can be considered the most feasible approach to keep computing time low [14]. In this study, the mixed liquor has been defined as a single-phase non-Newtonian fluid.

On the other hand, the Eulerian approach is the most commonly used in multiphase gas-liquid flow in full-scale aeration tanks. Comparing workability of different options in multiphase modelling, the other approaches available (Lagrangian particle tracking or Volume Of Fluid), despite being more accurate, are exceedingly expensive in terms of computing time and memory [15]. Population Balance Models (PBMs) represent a powerful modelling framework for the description of the dynamics of properties that are characterised by statistical distributions [16]. PBM applied to CFD can define the presence and the interaction of bubbles, based on break-up and coalescence models to reproduce the dispersed phase motion more correctly [17, 18].

Several two-phase flow (gas-liquid) CFD models have been developed over the last years focused on aeration of full-scale oxidation ditch configurations [2]. Multiphase modelling of AS tanks based on gas-liquid neutral density showed an overestimation of the mixing degree and its applicability to study bubbly bioreactors is still uncertain

[+] schiva@uji.es, Universitat Jaume I, Mechanical Engineering and Construction Department. Av. Vicent Sos Baynat, s/n 12071 Castellón (Spain). Telf: +34 964 728 141

[19]. The bubble size and the air hold-up are the parameters of paramount importance that govern the interfacial area. However, a fixed bubble diameter is commonly defined as an input without the code calculating the interfacial area density during the simulation. Moreover, the degassing approach is predominant [5, 6, 8, 11, 20, 21]. Unlike the other works mentioned and despite the high computational cost, the PBM and the free-surface approach has been used in this work to study the dispersed phase dynamics in detail including the liquid-air interface.

Usually, experimental data supplied to validate CFD models is relatively scarce due to the conflicting interests in terms of economics, time and complexity, especially in full-scale tanks studies. In addition to the determination of the overall fluid behaviour, CFD predictions need a detailed experimental validation since it provides very accurate results [22].

This paper shows a remarkable CFD modelling contribution through a comprehensive hydrodynamic analysis of an aerated tank, validated with local velocity measurements in 3D. The outline of this work was divided in three parts. Firstly, tracer tests are analysed to describe the global fluid behaviour. Subsequently, tracer results are related to the detailed description of the hydrodynamics provided by the CFD results. They were obtained for single-phase and two-phase flow models, depending whether the air is supplied or not. A valuable comparison of the two hydrodynamic regimes is shown in this section. Secondly, the experimental validation for both cases is discussed and then, the PBM results are analysed. Finally, the improvement of the hydraulic behaviour carried out using CFD modelling is shown.

2. Materials & methods

2.1 Description of the biological reactor

[+] schiva@uji.es, Universitat Jaume I, Mechanical Engineering and Construction Department. Av. Vicent Sos Baynat, s/n 12071 Castellón (Spain). Telf: +34 964 728 141

A full-scale biological reactor (WWTP La Union, Spain) of 7800 m3 composed of two symmetrical oxidation ditch units, wastewater treatment lanes (WWTLs), set in parallel, has been chosen for this study. The CFD model has been performed only in one of the tanks. The influent flow, about 1300 m3/day, and the external recycling arrive previously mixed into the inner channel (through the Inlet), which is expected to operate in anoxic conditions. Subsequently, fluid flow passes through the channel spacing (Fig. 1), which communicates both channels to the outer channel, leaving afterwards the biological reactor (Outlet) and going to the secondary settler tanks. The graphical description of the secondary treatment has been included in the supplementary material.

Mixing is provided by two submerged impellers (propellers) and the aeration diffuser system. The aeration area is divided in three grids of 153 diffusers (9 rows and 17 columns) located in the outer channel and installed at a height of 22cm (Fig. 1). The aeration is supplied following on-off cycles set by the ammonia concentration which is measured by a probe located at the outlet. As other works conducted in oxidation ditch configuration previously mentioned, the hydrodynamic and mixing conditions of the tank become even more important because simultaneous nitrification and denitrification is desired, as this case, at the outer channel, where both aerobic and anoxic conditions are present.

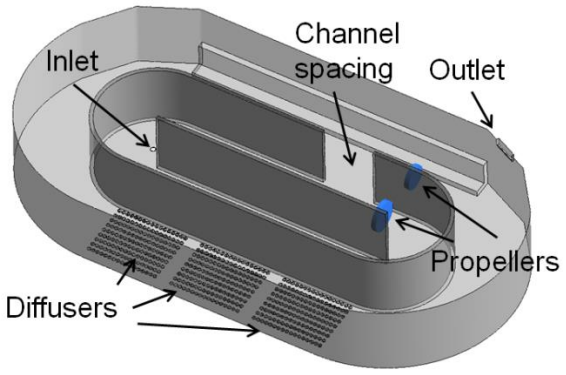

+ schiva@uji.es, Universitat Jaume I, Mechanical Engineering and Construction Department. Av. Vicent Sos Baynat, s/n 12071 Castellón (Spain). Telf: +34 964 728 141

Figure 1. 3D view of the full-scale model corresponding to WWTL1

2.2 CFD Modelling

The CFD models used in this study have been implemented by using the *ANSYS*® *Academic Research Release 16.2*. Two steady-state models have been implemented: a single-phase model representing the hydrodynamic conditions when the aeration is off, and a two-phase model to represent the flow hydrodynamic conditions when the aeration is on.

Tracer tests were used to enrich the definition of the boundary conditions, mainly the influent flow rate entering the 3D domain. Then, after the calibration of the thrust of the propellers, the CFD models were widely validated through the comparison of the experimental data using 3D fluid velocity profiles. Finally, different configurations were studied through new CFD models, based on changing the position of the propellers, to obtain an improved hydraulic configuration.

2.2.1 Single-phase

During the non-aeration stage the flow within the aeration tank can be accurately described by a single-phase model. The mixed liquor was modelled as an incompressible non-Newtonian Herschel-Bulkley fluid. The fitting parameters [23] were τ_0= 0.00883 □□; K= 0.01932 □□ □□; □=0.6262. Turbulence was modelled by using the Shear Stress Transport model [24] with automatic near-wall treatment. On the one hand, the SST turbulence model used consists on a two-equation eddy-viscosity turbulence model that combines the k-ω turbulence model near the wall

+ schiva@uji.es, Universitat Jaume I, Mechanical Engineering and Construction Department. Av. Vicent Sos Baynat, s/n 12071 Castellón (Spain). Telf: +34 964 728 141

when the inner region of the boundary layer has a dominant effect and k-ε turbulence model in the free shear flow. On the other hand, the automatic near-wall treatment implemented permits a consistent transition between regions with coarse meshes, where the viscous sublayer is modelled using the scalable wall functions developed by ANSYS [25], to regions with fine meshes, where the viscous sublayer can be fully resolved as long as 10 nodal points fall within it.

The tank walls were set as smooth non-slip walls, whereas the water surface was set as a free-slip wall. Inlet condition was set from the influent mass flow rate entering the domain normal to the inlet surface. The mass flow rate at the outlet boundary condition was set to the same value. The reference pressure was set to atmospheric pressure at the air water interface.

Regarding the implementation of the propellers, the momentum source approach was used. Here, the propeller geometry is replaced by a cylindrical subdomain containing a momentum source driving the fluid movement. The corresponding volumetric momentum source, M (kg m^{-2} s^{-2}), can be calculated as

$$M = \frac{F}{V_{cyl}} \left(\frac{q}{D}\right)^2, \qquad (4)$$

D being the diameter of the stirrer (m), ρ the fluid density (kg m^{-3}) and V_{cyl} (m^3) the volume of the cylindrical subdomain. The flow rate propelled, q (m^3/s), can be obtained as

$$F = C\,q \left(\frac{q}{D}\right)^{\frac{1}{2}}. \qquad (3)$$

In this equation, *F* stands for the thrust force (N) and *C* is constant parameter related to the propeller efficiency, depending on several factors such as the tank geometry or flow configuration.

+ schiva@uji.es, Universitat Jaume I, Mechanical Engineering and Construction Department. Av. Vicent Sos Baynat, s/n 12071 Castellón (Spain). Telf: +34 964 728 141

In practice, technical sheets provided by propeller manufacturers include values for the stirrer diameter and thrust force, whereas the parameter *C* must be adjusted in the model so that the flow rate in the tank matches the experimental one. In the present case, the parameter C was calibrated for each propeller, fitting the average velocity calculated at two sections of the channels of the tank with the experimental data. Unlike other authors [26], the swirling flow effect was not implemented separately, it was assumed to be included implicitly in the calibration of the momentum source of the propeller. As a result, the internal propeller was represented by a thrust force of 1750 N, a blade diameter of 2.5 m, and C=0'875. With respect to the outer diameter, the force was 1750 N, with a blade of 2 m and C=0.875. As subdomains, the cylinder diameters were set equal to the corresponding blade diameters, with a cylinder length of 0.4 m. The momentum sources resulted in 300 and 440 kg m^{-2} s^{-2}, respectively.

2.2.2 Two-phase flow

The effects of the air injection significantly change the flow hydrodynamics when the aeration is turned on. Momentum transfer from bubble swarms have a clear influence on the velocity field of the mixed liquor, especially in the region located right on the top of the aerators. This simulation has been set up accurately to account for these hydrodynamic changes focusing on the modelling of the diffusers and the free surface. Also, the oxygen in the air bubbles is transferred to the mixed liquor. Given the dimensions of the domain and the huge number of bubbles to be implemented, the two-phase Eulerian-Eulerian framework was selected to account for these two effects in the CFD model.

The dispersed phase was modelled as a polydispersed incompressible gas with a zero-equation model for the turbulence. The homogeneous MUSIG framework [27] was used to account for the distribution size. In this approach, the dispersed phase is

+ schiva@uji.es, Universitat Jaume I, Mechanical Engineering and Construction Department. Av. Vicent Sos Baynat, s/n 12071 Castellón (Spain). Telf: +34 964 728 141

divided into M groups with given particle sizes. The fraction of particles that fall into each group (size fraction) is determined at the dispersed phase inlet, i.e. one must stablish the size distribution produced by the diffusers. Then, a set of PBM equations is applied to compute the size fractions of each group considering the inter-fraction mass transfer which results from bubble coalescence and breakup. In the proposed simulations, 10 groups with sizes uniformly distributed between 1 and 10 mm bubble diameter were defined, for example, Group 1 corresponded to 1mm bubble size and so on. Break-up was introduced by using the model [28]. The coalescence model is based on the Prince and Blanch frequency calculation [29], which is based on a kinetic model applied to molecular collisions. This base frequency is multiplied by the

a) Wu correlation [30], to account for the size of the bubbles that collide, and
b) Wang correlation [31], to account for the finite length of the eddies driving the collisions.

With respect to the boundary conditions, tank walls were introduced as free-slip walls for the dispersed phase, and non-slip condition for the liquid phase.

Regarding the inlet, let us recall that a total air flow-rate of 990 Nm3/h was injected equitably by the 459 disc diffusers (3 grids of 153 diffusers each). So each diffuser was modelled as an air inlet boundary condition, providing the specified mass flow rate. To complete the boundary condition, the hold-up at the inlet was computed as

$$\alpha = \frac{Q_{air}}{A_{diff} v_b}. \qquad (3)$$

Where v_b stands for the terminal velocity corresponding to 3 mm air bubbles in clean water which was calculated using [32] Jamialahmadi correlation resulting 0,25 m/s and A_{diff} represents the diffuser area equals to 0,039 m^2, corresponding to 0,023 m and 0,050 m for the external and the internal diffuser diameter, respectively. Given these conditions in the setup, the inlet hold-up resulted in a 5.65 %.

+ schiva@uji.es, Universitat Jaume I, Mechanical Engineering and Construction Department. Av. Vicent Sos Baynat, s/n 12071 Castellón (Spain). Telf: +34 964 728 141

Note that, unlike previous works mentioned which injected air through the total surface of the diffuser, in this simulation the diffusers were drawn in detail with 3D CAD software to introduce air only through the perforated annular area. This increased considerably the total number of nodes of the mesh compared to the single-phase model, from 1,910,099 to 2,927,830. The modelling of the free surface made it necessary to increase the 3D domain in the vertical direction by 0.5 m, introducing a mesh refinement to reproduce the interface liquid-gas interface. This gave a more detailed description of these two regions that is extremely important to describe the dispersed phase correctly. The meshes for the simulations were selected following the CFX Best Practices Guide for Numerical Accuracy. Tetrahedral dominant meshes were performed to calculate the simulations which guarantee the accuracy and stability of the numerical computation by the mesh quality parameters (Aspect ratio and Skewness). These details have been included as supplementary material.

To model the liquid phase, the rheological conditions from the single-phase model were preserved. Also, the SST model was used for the turbulence modelling. The same boundary conditions as in the single-phase case were used, except for the water surface. In this configuration, the water-air surface was modelled by means of a free-surface model [33] instead of the degassing approach used in the references included in this work. The displacement of the liquid level caused by the injection of the air is thus accurately reproduced, leading to a better description of the flow in the regions surrounding the aerators. The top surface of the domain was set as an opening to the atmosphere.

Let us recall that the simulation of multiphase flows is generally quite complex as it involves not only the computation of the conservation equations fields for each phase, but also the interaction between the two phases (momentum and mass transfer). For

[+] schiva@uji.es, Universitat Jaume I, Mechanical Engineering and Construction Department. Av. Vicent Sos Baynat, s/n 12071 Castellón (Spain). Telf: +34 964 728 141

the interface forces, we have considered the Ishii-Zuber drag correlation [34], the Favre Averaged turbulent dispersion [35], and the Sato correlation for bubble induced turbulence [36, 37]. Lift and wall force were implemented following [38].

2.3 Experimental measurements

CFD models need global and, where possible, local measurements in order to become a robust simulation tool. An exhaustive validation campaign was conducted by means of 3D velocity measurements. Moreover, tracer tests were carried out to understand the global fluid behaviour, to identify defects of the fluid and to define the boundary conditions for the CFD models, mainly the influent flow rate.

2.3.1 Tracer test

The main purpose of the tracer test carried out in this study was to obtain the flow pattern and define the hydraulic distribution of the flow entering the two lanes (WWTL1 and WWTL2). This allowed the influent flowrate to be defined for the one-tank CFD model correctly (WWTL1). Since the flow meters are located after the secondary treatment and there was no fine control of the flow entering each lane, a comparative study between both oxidation ditch lanes allowed the distribution of the flow to be quantified. Moreover, the mean residence time and the number of tanks-in-series was calculated, and the absence of important defects of the fluid was verified [39]. Additionally, some typical features of the tracer response curves analysis were discussed. Finally, some singularities of the mixing observed in the inner channel were analysed and compared with the CFD results.

[+] schiva@uji.es, Universitat Jaume I, Mechanical Engineering and Construction Department. Av. Vicent Sos Baynat, s/n 12071 Castellón (Spain). Telf: +34 964 728 141

The tracer technique was carried out obtaining the tracer response curve in several points during 10 days (about 2 * τ) [40] where 225 samples were taken over the course of the secondary treatment. The tracer was diluted in 50 litres of tap water and added using a "pulse" injection of 18 seconds. Fluorescein sodium salt was selected as the dye tracer and the samples were processed with a fluorescence spectrophotometer Varian Cary Eclipse. Finally, the tracer test was validated satisfactorily by means of a tracer mass balance, which showed a deviation within an acceptable range considering the complexity of performing this experimental technique at full-scale. From the accuracy of the instrumental equipment and the measurements, we estimated that the error in the concentration values is not higher than 5%, which allowed us to provide reliable values for the results. The information about the performance of the tracer tests has been included as supplementary material.

2.3.2 Fluid velocity profiles

Despite the fact that tracer tests can be used as a global validation technique for the CFD model, fluid velocity profile measurements are preferred because they provide a detailed and local hydrodynamic analysis in 3D.

The aim of the extensive sampling campaign was to obtain a comprehensive hydrodynamic analysis of a full-scale oxidation ditch and validate the CFD models. Special efforts were made to characterise the fluid behaviour within the channel spacing due to the tank's difficult accessibility. This was considered the most important critical zone, the zone from which one can obtain crucial information about the fluid behaviour due to the magnitude of the flow activity. 3D fluid velocity profiles were determined experimentally at several points along the tank at 14

[+] schiva@uji.es, Universitat Jaume I, Mechanical Engineering and Construction Department. Av. Vicent Sos Baynat, s/n 12071 Castellón (Spain). Telf: +34 964 728 141

positions and 3 heights without aeration, and 7 positions and 3 heights with aeration on.

A high-resolution acoustic doppler velocimeter *Vectrino Nortek*® was used to measure the fluid velocity components at 25Hz within a sampling volume of 7 mm length. The total time of sampling for each measurement was 300s to capture large eddies. Then, the raw signals acquired by the equipment were treated using a Savizky-Sgolay filter to smooth the signal. The instrument, which has an error of ±1 mm/s, proved to be appropriate for this purpose although measurements over the diffusers were avoided due to the difficulties of the equipment to measure in bubbly flow. As a consequence, measurements with gas had to be carried out before and after the grids and then to apply a depickling [41].

An aluminium structure of 4.5 meters, made of four pieces of 3-point-truss of 1.5 m each, was anchored to the walls. A mobile wagon was made to slide over this structure driven by a pulley system in order to set the position over the surface of the tank. An aluminium profile of 9 m was attached vertically to the wagon as a guide for the velocimeter. Thus, the velocimeter was able to move automatically at different heights actioned by a stepper motor. This system allowed the movement of the velocimeter with enough precision inside the tank to measure 3D fluid velocity at different locations and depths.

3. Results & Discussion

3.1 Tracer test

Analytical methods related to the residence time distribution are very useful to characterize the hydraulics and macroscopic mixing, in an integrated way with no

[+] schiva@uji.es, Universitat Jaume I, Mechanical Engineering and Construction Department. Av. Vicent Sos Baynat, s/n 12071 Castellón (Spain). Telf: +34 964 728 141

spatial information but are able to determine reactor malfunctioning flows such us short-circuiting or dead volume [42], which is especially important in large-volume tanks.

Figure 2 shows the tracer concentration-time experimental data, C(t), obtained at the Outlet (Outlet 1 and Outlet 2) corresponding to both WWTLs working in aeration cycles for 10 days. This showed that in general, both lanes corresponded to a similar hydrodynamic performance noticing that the overall flow behaviour is related to a mixed flow, and the maximum concentration of tracer was achieved in a similar time (4h and 6h, for WWTL1 and WWTL2, respectively). It showed an exponential decay of C(t) which corresponded to completely stirred tank reactor (CSTR) with a reasonably good flow where an adequate mixing can be assumed [39]. The time lag (initial time) can be neglected even though the path the flux must travel from the inlet to the outlet. It is important to mention that, though the global hydrodynamic behaviour of the fluid was favourable, defects in the extent of mixing were detected, especially after achieving the time of maximum tracer concentration. The separate flow analysis of the inner channel allows to better understand the fluid behaviour of the whole tank.

[+] schiva@uji.es, Universitat Jaume I, Mechanical Engineering and Construction Department. Av. Vicent Sos Baynat, s/n 12071 Castellón (Spain). Telf: +34 964 728 141

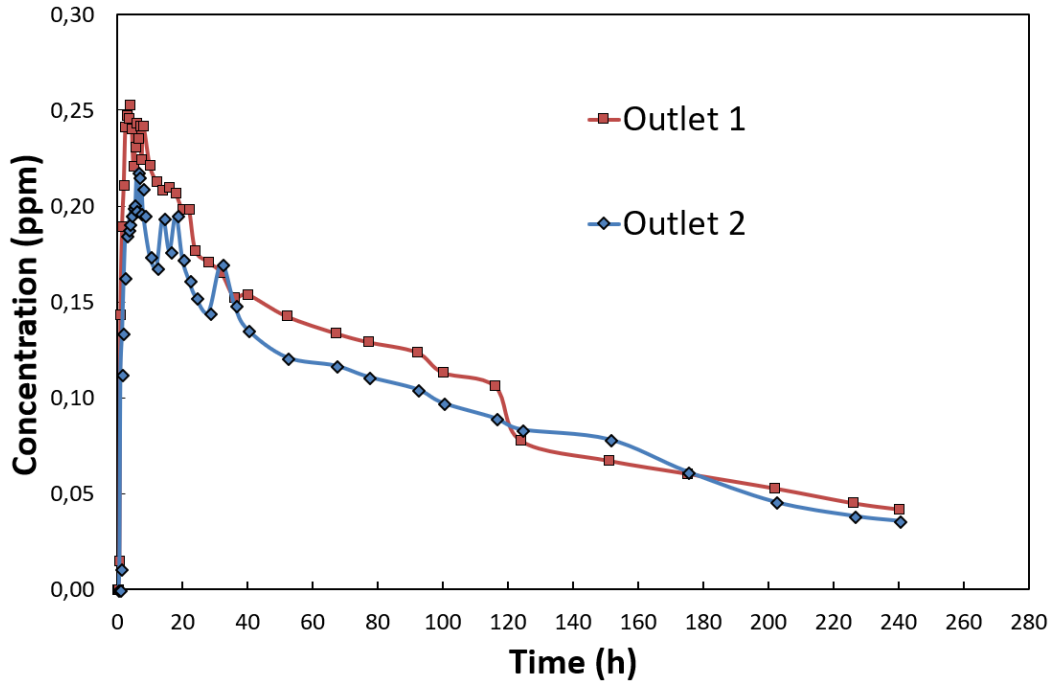

Figure 2. Concentration vs time tracer response curves obtained at the Outlet

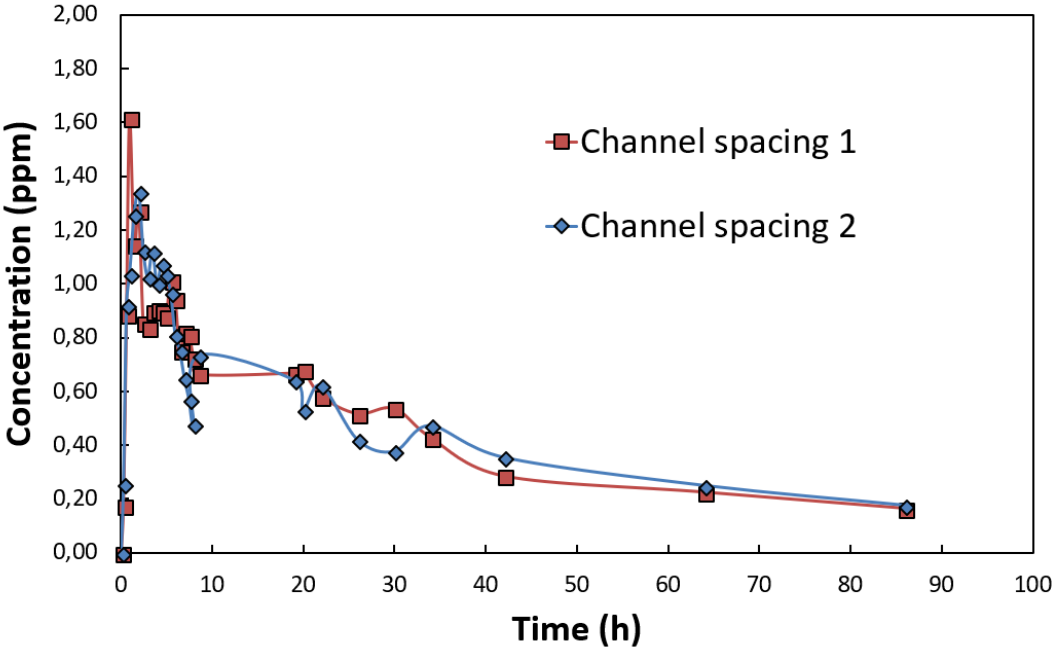

Figure 3. Concentration vs time tracer response curves obtained at the Channel spacing

[+] schiva@uji.es, Universitat Jaume I, Mechanical Engineering and Construction Department. Av. Vicent Sos Baynat, s/n 12071 Castellón (Spain). Telf: +34 964 728 141

Figure 3 shows the tracer concentrations measured at the channel spacing of both lanes, which allows the inner channels to be analysed separately. The tracer concentrations revealed a slow internal circulation within the inner channel of both lanes which suggested inadequate mixing where portions of reactor contents may not mix with the incoming water [4]. This was caused by the faulty propeller positioning in the inner channel. This caused some singularities of the fluid behaviour which were analysed in depth and compared to the CFD model. They have been included as supplementary material.

Mean residence time (t_m) can be calculated either from C(t) or residence time distribution E(t) following the equation 1. To do this, the C(t) curve was fitted with a single-term exponential function (refer to supplementary material). Since the distributions pointed out the flux behaviour corresponded to a CSTR, the number of tanks-in-series (N) was calculated for both WWTLs using the variance σ^2 from the equation 3 [36] as well as some indices to characterise the flux [39]:

$$\square_{\square} = \frac{\int_0^{\infty} \square\,\square(\square)\,\square\square}{\int_0^{\infty} \square(\square)\,\square\square} = \int_0^{\infty} \square\,\square(\square)\,\square\square \quad (1)$$

$$\sigma^2 = \int_0^{\infty} (\square - \square_{\square})^2 * \square(\square)\,\square\square \quad (2)$$

$$\square = \frac{\square_{\square}^2}{\square^2} \quad (3)$$

Both bioreactors showed the $\square_{\square}$ value close to the theoretical hydraulic retention time, τ, did not present remarkable defects in the fluid behaviour. On the one hand, both C(t) curves measured at the Outlet did not show presence of short-circuiting since the expected initial concentration of 0.25 mg/l matched with the maximum concentration

+ schiva@uji.es, Universitat Jaume I, Mechanical Engineering and Construction Department. Av. Vicent Sos Baynat, s/n 12071 Castellón (Spain). Telf: +34 964 728 141

measured. On the other hand, an indicator of dead volume percentage, θ_d , was calculated as the deviation of θ_d from τ , as $\theta_d = (1 - \frac{\theta_d}{\tau})$. Table 1 shows the other indices calculated. The reactor dispersion Index (MDI), was calculated as the ratio of t_{90}/t_{10}, relating the passage of 10% (t_{10}) and 90% (t_{90}) of the mass through the Outlet. It confirmed that the global fluid behaviour corresponded to a completely mixed flow rather than plug flow (MDI values up to 22 correspond to CSTR behaviour while MDI value less than 2 is related to an effective plug-flow reactor) 5 The number of tanks in series resulted less than 2 for each WWTL. Moreover, a slightly unequal distribution of the flowrate entering the WWTLs was determined based on the total mass tracer concentration measured in both C(t). Thus, a deviation of 5% in the ratio of both θ_d was calculated, which can be understood as the WWTL1 processed a slightly higher flowrate than WWTL2. This assumption was also supported in that the maximum concentration was detected earlier in WWTL1 at both C(t) curves. It also justifies the high θ_d value obtained for WWTL1 since its calculation was based on the τ. Further information about the tracer test characterization has been included as supplementary material.

Table 1. Indices calculated in C(t) tracer response curves obtained at the Outlet

Case	τ (day)	θ_d (day)	θ_d (%)	t_{10} (h)	t_{90} (h)	t_{90}/t_{10}	σ^2 (day^2)	N
WWTL1	6.16	5.69	7.63	11	175	15.91	8.11	1.82
WWTL2	6.16	5.98	2,92	12	175	14.56	8.02	1.94

+ schiva@uji.es, Universitat Jaume I, Mechanical Engineering and Construction Department. Av. Vicent Sos Baynat, s/n 12071 Castellón (Spain). Telf: +34 964 728 141

The oxidation ditch configuration studied avoids the presence of short-circuiting due to the path the fluid must travel to get to the outlet from the inlet. Although this configuration seems to be more plug-flow because of its geometry distributed in two channels, the hydraulic behaviour indices indicate a marked CSTR behaviour, which will be increased as t_m increases.

3.2 CFD models

This section shows the results of the different CFD models performed to investigate the hydrodynamic behaviour of this oxidation ditch configuration. Firstly, the hydrodynamics will be analysed through CFD results. Secondly, the single-phase CFD model will be validated by comparing the 3D fluid velocity profiles calculated with the experimental data. Finally, in the same way, the two-phase flow CFD model results will be validated, and the PBM results will be used to go in depth in the aeration performance.

3.2.1 Hydrodynamic performance of the oxidation ditch

Figure 4 shows the velocity field within the tank by means of the streamlines. In general, a more homogeneous fluid velocity distribution and a higher average fluid velocity resulted for the configuration without air. Even so, the maximum fluid velocity corresponded to the regions over the diffuser grids for the configuration with air, specifically, the region placed at the top and located immediately behind the third grid following the fluid direction at the outer channel. In both cases, the lowest velocity zones took place in the inner channels. This was caused by the faulty positioning of the propeller, placed too close to the internal curved wall. Thus, the

[+] schiva@uji.es, Universitat Jaume I, Mechanical Engineering and Construction Department. Av. Vicent Sos Baynat, s/n 12071 Castellón (Spain). Telf: +34 964 728 141

curved wall guided the current round, which cannot be impelled perpendicularly by the internal propeller, deflecting the plume driven by the propeller. Consequently, a considerable entrainment of the current flow through the channel spacing from the outer to the inner channel was induced, promoting the malfunctioning of the inner channel. This can be appreciated in Figure 5.

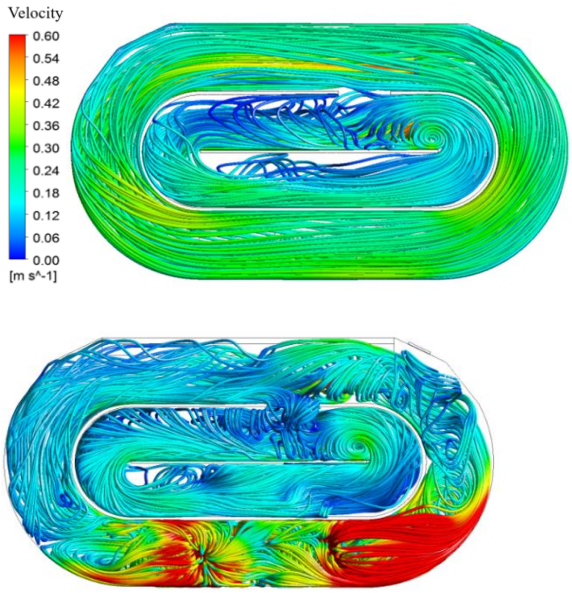

Figure 4. Velocity of the streamlines without air (left) and with air (right)

Figure 5 shows the velocity field contours plotted at five different height cross sections. Some vectors, equally spaced, were added to better understand the fluid direction. The case without air showed a more homogeneous velocity field, well balanced throughout the domain, and strongly governed by the driving force of the propellers. Comparing the effect of the plumes induced by the propellers at the 1.5m and the 2.5m high velocity contours, the external propeller exhibited a favourable performance while the internal propeller did not work as expected. As described previously, its plume was altered, and the flux was guided to the centre wall, generating regions with slow internal circulation of the flux and recirculation effect. This can be appreciated by the direction of some vectors plotted over the low velocity

[+] schiva@uji.es, Universitat Jaume I, Mechanical Engineering and Construction Department. Av. Vicent Sos Baynat, s/n 12071 Castellón (Spain). Telf: +34 964 728 141

regions. For the case with air, the velocity field was more inhomogeneous, especially after the grids in the direction of the fluid flow, which was mainly influenced by the air injection. Thus, the leading role of the external propeller over the hydrodynamics in the outer channel decreased considerably. The air injected generates a convective cell of fluid, providing the maximum fluid velocity over the diffusers and contributing notably in the reduction of the average fluid velocity along the outer channel. Moreover, the convective cell generates an appreciable recirculation flow effect in the curved region after the diffuser grids, over the full height, reinforced by the effect of the fluid meeting the external curved wall at maximum velocity. The convective cell induced by the raising bubble columns will be analysed in depth in section 3.2.4.

In both cases, there was an unintended high flow exchange between channels. Hence, the way to reduce the flow entering through the channel spacing will be calculated in section 3.3.

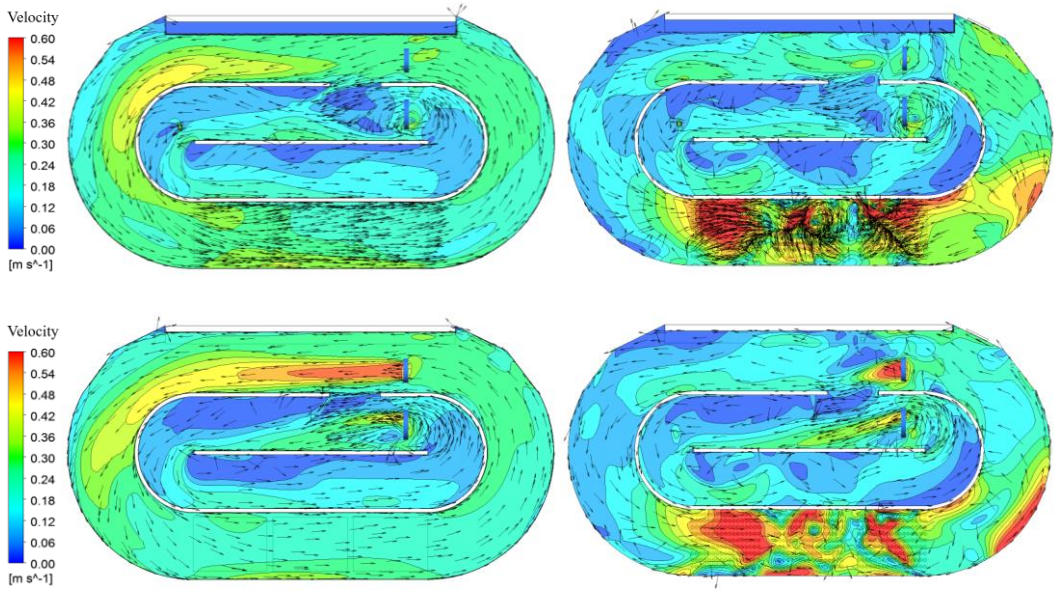

+ schiva@uji.es, Universitat Jaume I, Mechanical Engineering and Construction Department. Av. Vicent Sos Baynat, s/n 12071 Castellón (Spain). Telf: +34 964 728 141

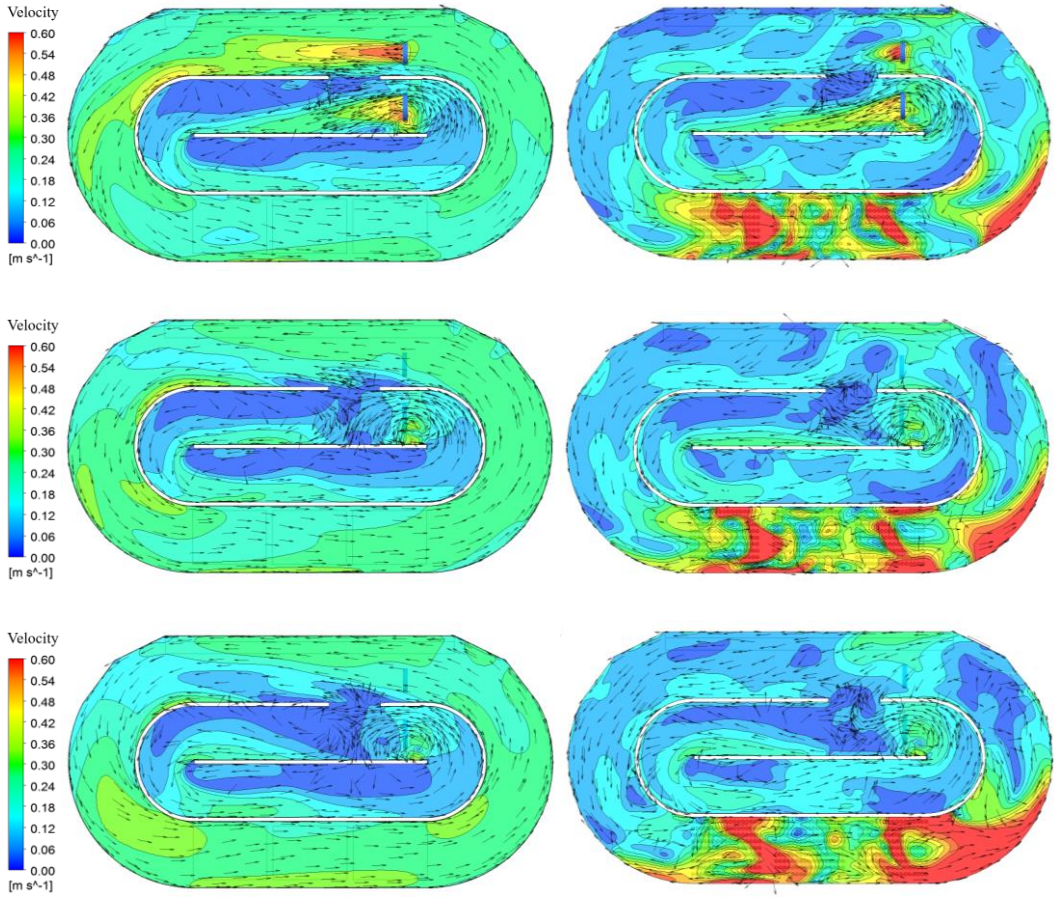

Figure 5. Velocity contour at 0,5 m, 1,5m, 2,5m, 3,5 and 4,5m high (from top to bottom) without air (left) and with air (right)

Figure 6 shows the five vertical fluid velocity profiles (P1, P2, P3, P4 and P5) selected to explain graphically the functioning of the hydrodynamics around the outer channel together with figure 5. As shown, they were positioned in the centre of the outer channel and distributed along the direction of the current flow from the external propeller. Importantly, for a given vertical section of the outer channel (5,54 m wide and 5,4 m high), the vertical fluid velocity profile changes in 3D across the width as will be shown in sections 3.2.2 and 3.2.3. That said, the five fluid velocity profiles corresponded to the modulus of the fluid velocity; they were considered enough representative of their sections to carry out the following flow analysis. Figure 6 shows the flow pattern along the channel. For the case without air, the closer the fluid

+ schiva@uji.es, Universitat Jaume I, Mechanical Engineering and Construction Department. Av. Vicent Sos Baynat, s/n 12071 Castellón (Spain). Telf: +34 964 728 141

was to the propeller, the more pronounced was the vertical fluid velocity profile. Thus, P1 showed the maximum velocity values around 2m high, where the external propeller was located. Since the flowrate is conservative along the outer channel and the section is constant, the fluid velocity profile must be balanced inside each section. According to this, at the top, P1 also presents the minimum fluid velocity values. Subsequently, the velocity profiles flatten as they move away from the external propeller. Thus, P4 exhibited a total flat vertical velocity profile while the suction effect of the propeller was appreciated through P5, located behind it. As expected from figure 5, figure 6 showed a more inhomogeneous vertical velocity profiles for the case with air, where P3 presented the maximum velocity values at the top and P1 was less pronounced compared to the case without air.

The average flowrate through the outer channel was evaluated at five sections corresponding to P1 – P5 (Fig. 6). The same value resulted for each section, with an error less than 0.25%, validating the conservation of the mass. Comparing both cases simulated, without and with air, the average velocity calculated was 0,249 m/s and 0,098 m/s correspondingly. Hence, the average flowrate circulating inside the outer channel reduced by 60% when the aeration was supplied. Furthermore, it is important to highlight that the hydraulic influence of the influent over the internal fluid behaviour can be neglected since the influent flowrate entering the tank was compared with the flowrate circulating internally in the channel, representing less than 1%.

[+] schiva@uji.es, Universitat Jaume I, Mechanical Engineering and Construction Department. Av. Vicent Sos Baynat, s/n 12071 Castellón (Spain). Telf: +34 964 728 141

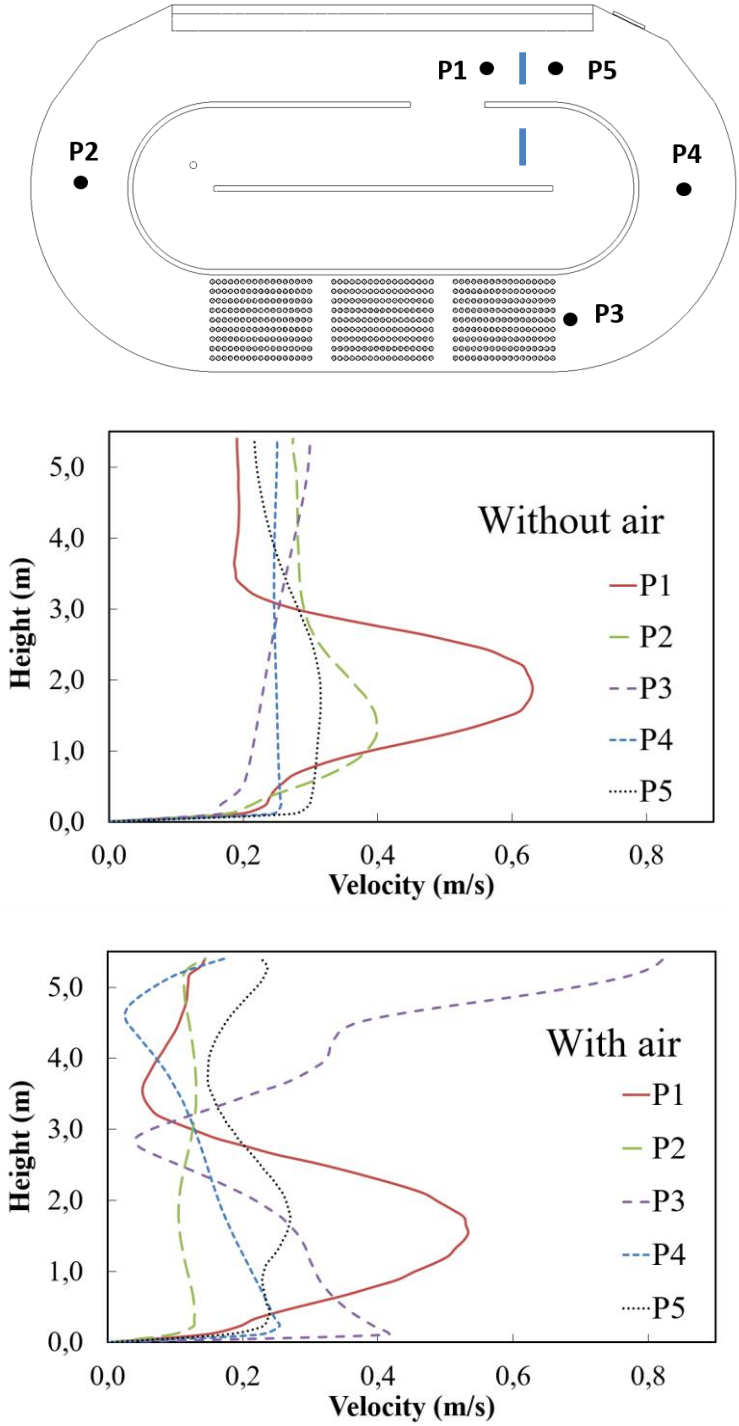

Figure 6. Vertical velocity profiles around the outer channel (P1 – P5) without and with air.

3.2.2 Single-phase CFD model validation

+ schiva@uji.es, Universitat Jaume I, Mechanical Engineering and Construction Department. Av. Vicent Sos Baynat, s/n 12071 Castellón (Spain). Telf: +34 964 728 141

Figure 7 shows the experimental measurements performed to validate the single-phase simulations. It shows the (x, y and z) velocity components compared to the CFD simulation results. The figure includes the graphical scheme in the X, Y plan view and the legend of the velocity components. The 14 positions of the measuring points were spread all over covering each of the critical zones of the tank and the width dimension of the channel. Thus, 3 different heights were measured in each position which gives a total of 42 measurements. The left axis of the figures shows the height (m) from the bottom to the top, which corresponds to the Z axis.

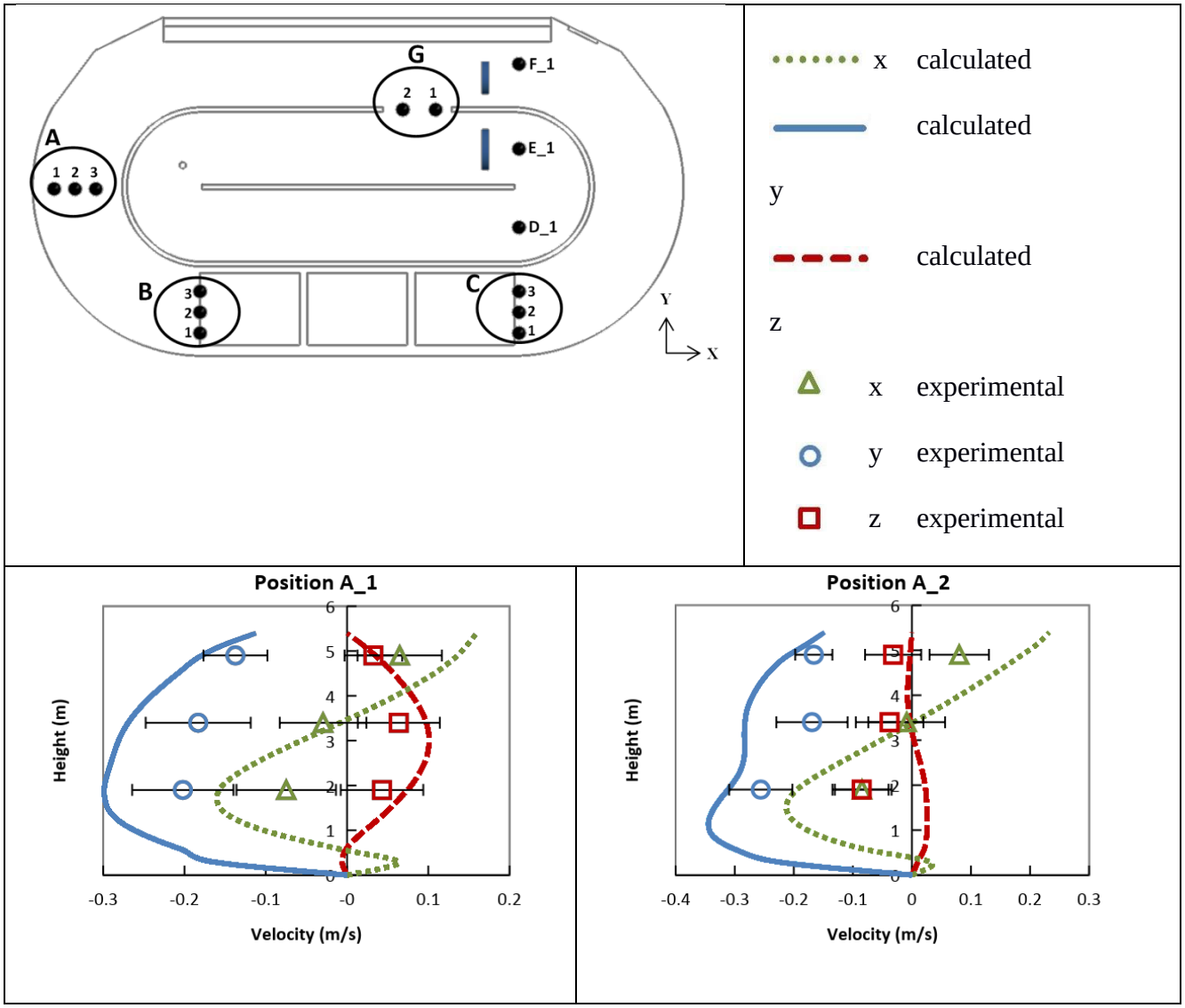

+ schiva@uji.es, Universitat Jaume I, Mechanical Engineering and Construction Department. Av. Vicent Sos Baynat, s/n 12071 Castellón (Spain). Telf: +34 964 728 141

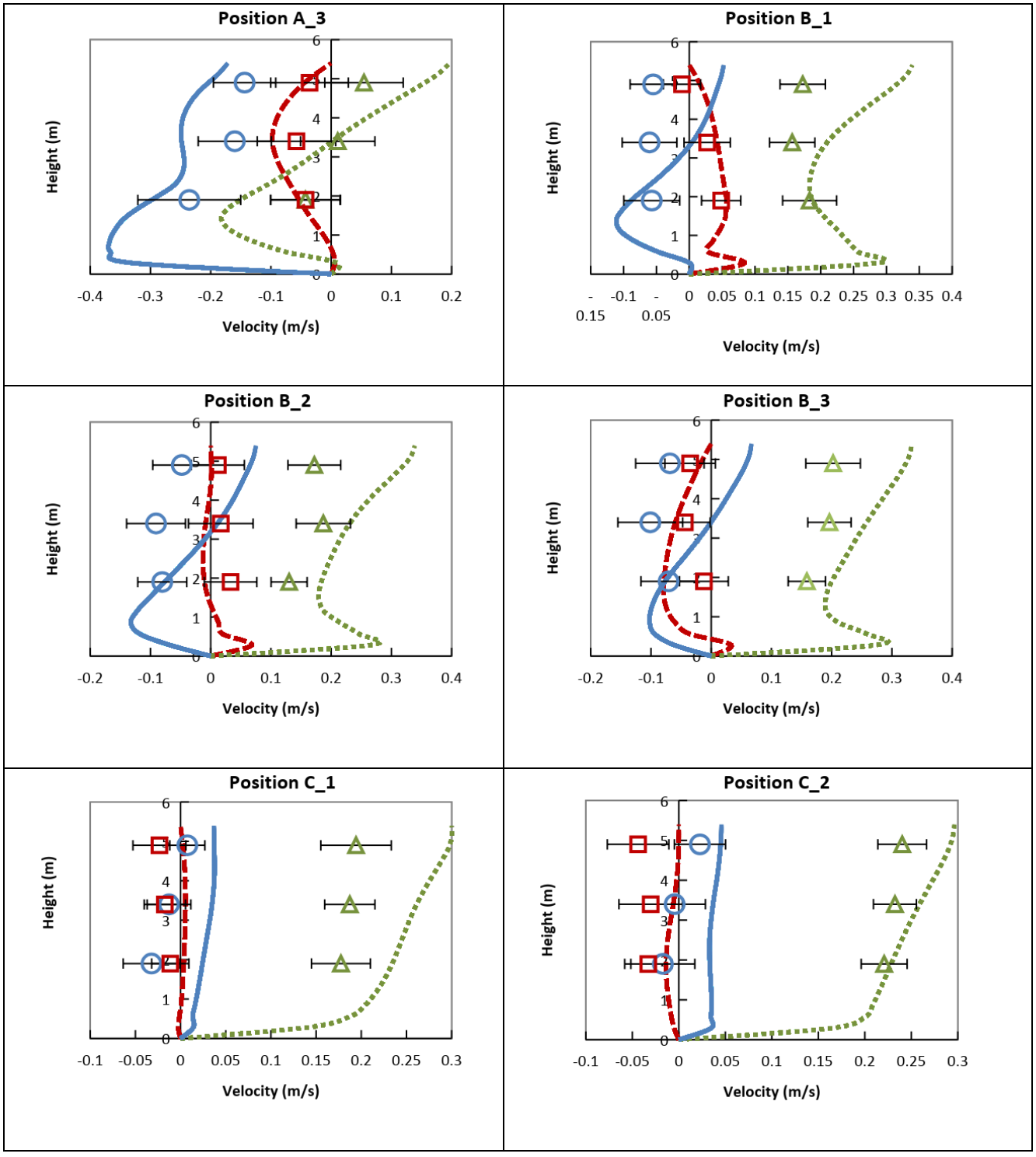

+ schiva@uji.es, Universitat Jaume I, Mechanical Engineering and Construction Department. Av. Vicent Sos Baynat, s/n 12071 Castellón (Spain). Telf: +34 964 728 141

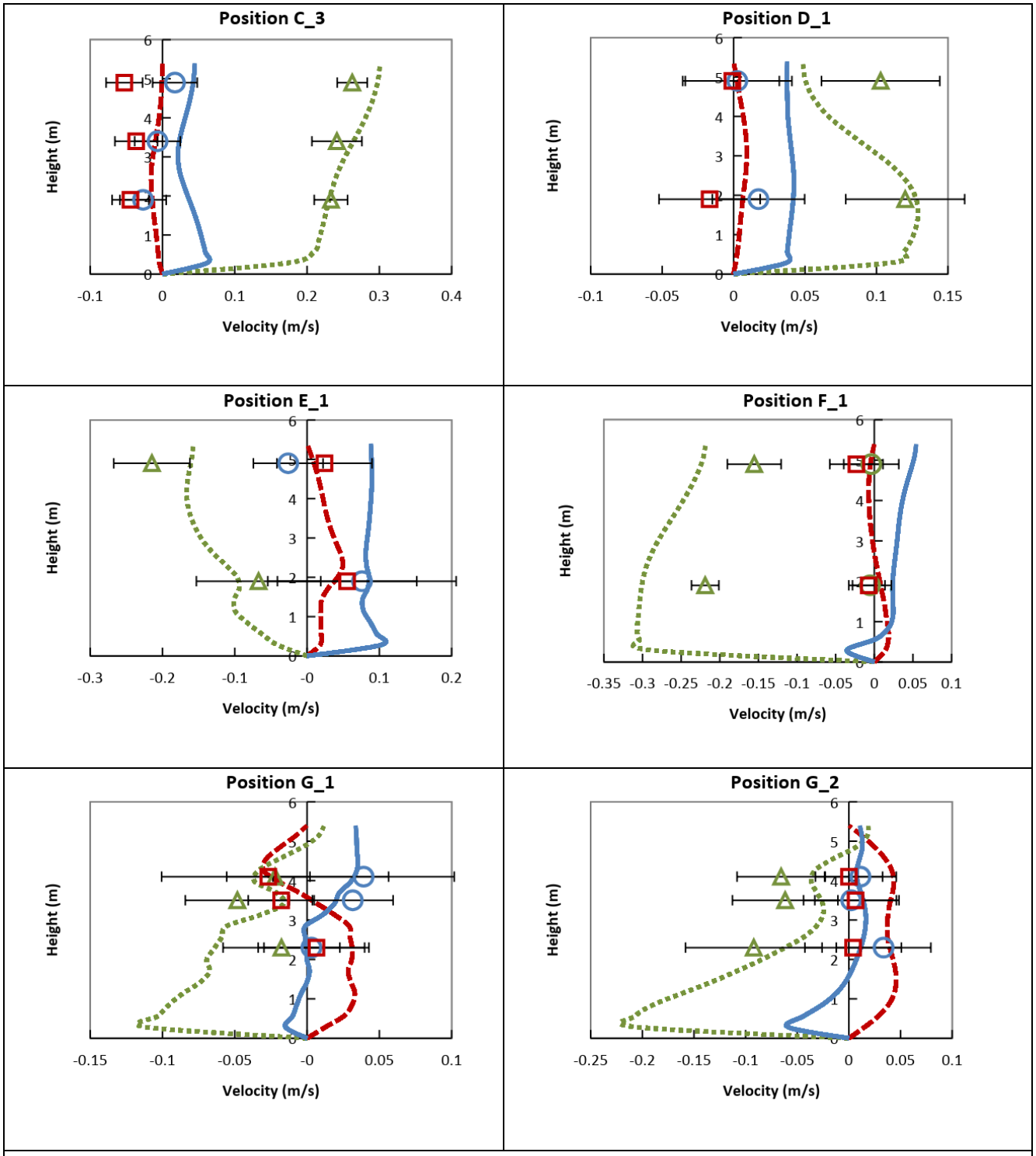

Figure 7. Comparison of the fluid velocity components calculated and measured without air.

In general, the results provided by the CFD model reproduced correctly the trends of the velocity in each component in all of the positions measured. The distribution of the fluid velocity components for the single-phase model depended considerably on

+ schiva@uji.es, Universitat Jaume I, Mechanical Engineering and Construction Department. Av. Vicent Sos Baynat, s/n 12071 Castellón (Spain). Telf: +34 964 728 141

the geometry of the tank and as previously analysed, on the relative distance of the position from the propellers. Thus, the 3 positions located in A and B presented the velocity components distributed in the directions X and Y due to the influence of the curved wall of the tank. Hence, Position A showed the maximum velocity values in Y while position B in X. In both positions, the fluid velocity profiles are more pronounced at 2 m height where the propeller is located. Conversely, position C presented only one velocity component as the predominant, in X direction, due to the straighter geometry which influences the flow stream. As previously explained, the suction effect of the propeller can be appreciated in position F comparing the velocity component in X to the position C. Although the diameter of the internal propeller is higher, and the section of the inner channel is lower than the outer channel, the experimental measurements performed in the positions D and E reveals lower fluid velocity. It was reproduced with high accuracy by the CFD model. Finally, it is important to highlight the difficulty of performing the velocity measurements in position G and to describe the fluid behaviour in 3D through the Channel spacing (refer to the supplementary material).

The average velocity is a more common way to fit the experimental measurements by the CFD model, which tends to reduce the error for validation. This work attempts to reproduce the fluid velocity, component by component in each measuring point, to provide a very detailed performance which is a more difficult way to agree with the experimental data. It is often tedious to locate the velocimeter with high accuracy in the full-scale tank and matching the same position in the 3D CFD model to evaluate their results with the experimental data. The error bar was included as the standard deviation associated to the experimental measurements. In order to provide a quantitative measurement for the quality of the simulation, the experimental dataset

[+] schiva@uji.es, Universitat Jaume I, Mechanical Engineering and Construction Department. Av. Vicent Sos Baynat, s/n 12071 Castellón (Spain). Telf: +34 964 728 141

was compared to the corresponding values in the simulation through a linear regression. The resulting root mean squared error was found to be 0.048 m/s, with a coefficient of determination (R^2) of 0.88 [43].

3.2.3 Two-phase flow CFD model validation

As in the previous section, figure 8 shows the experimental measurements with air performed in 7 positions to validate the two-phase CFD simulations. Following the same procedure of the single-phase measurements, 3 different heights were evaluated which gave a total of 21 measurements. It was also included a graphical scheme in the X, Y plan view and the legend of the velocity components. The left axis of the figures shows the height (m) from the bottom to the top, which corresponds to the Z axis.

The inner channel offered a similar fluid behaviour as the single-phase case because it was virtually not affected by the aeration. Thus, lower number of sampling points were evaluated, all them concentrated at the outer channel.

The results calculated for each velocity component reproduced correctly the general trend compared to the experimental data. As analysed in section 3.2.1, the experimental measurements performed with air in the position A, exhibited the reduction of the value of velocity, maintaining the distribution of the components but changing the vertical profile to flatter. As mentioned above, the characteristic plumes of the aeration and the vertical motion of the dispersed phase reduced the axial velocity of the mixed liquor circulating within the outer channel.

The plumes of air increase the free surface height which induces the acceleration of the flux at the top and causes the recirculation of the current flow before the grid zone. The backflow was observed along the free surface. Position B showed a marked profile of velocity component X, which changed drastically from negative values at the top to positive velocity values at the bottom. Conversely, position C showed high

+ schiva@uji.es, Universitat Jaume I, Mechanical Engineering and Construction Department. Av. Vicent Sos Baynat, s/n 12071 Castellón (Spain). Telf: +34 964 728 141

values of the x component in the direction of the current flow at the top, and negative values at the bottom, caused by the convective cell induced by the raising bubble columns.

As with the single-phase simulation, the goodness of the simulation was evaluated, obtaining a root mean squared error of 0.098 m/s (R^2=0.71). This error is significantly higher than the single-phase value, implying that the two phase models currently used need further development.

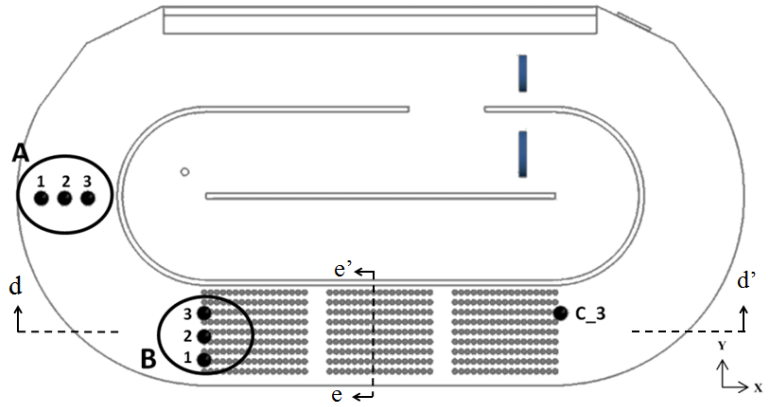

x calculated

calculated

y

calculated

z

x experimental

y experimental

z experimental

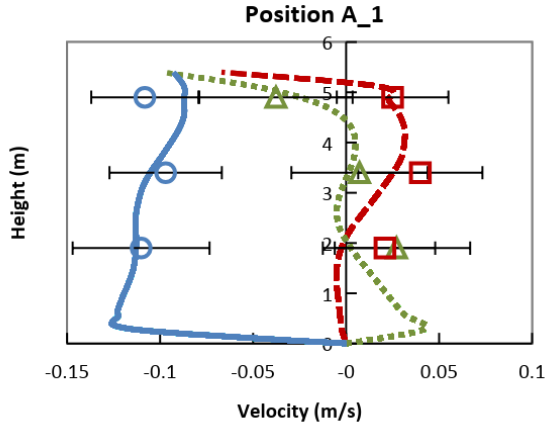

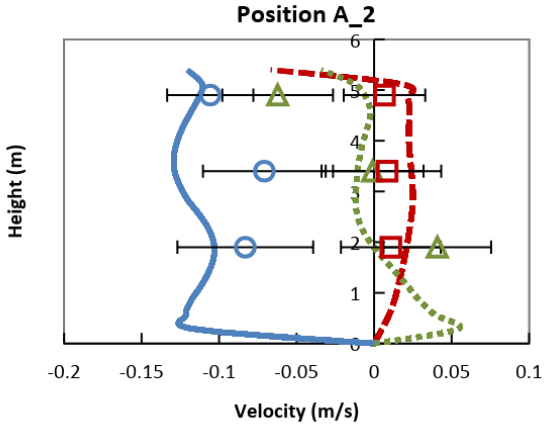

+ schiva@uji.es, Universitat Jaume I, Mechanical Engineering and Construction Department. Av. Vicent Sos Baynat, s/n 12071 Castellón (Spain). Telf: +34 964 728 141

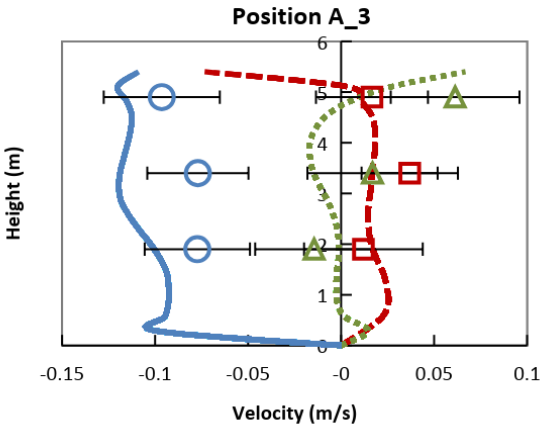

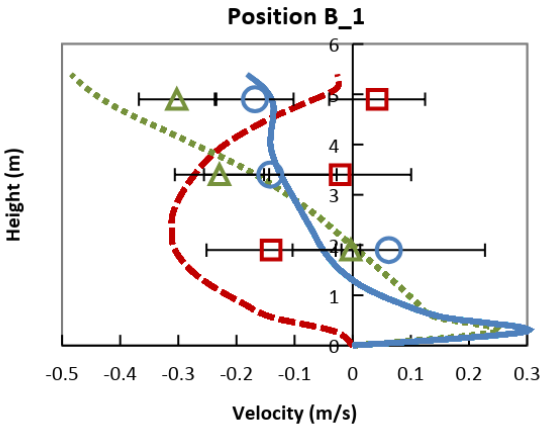

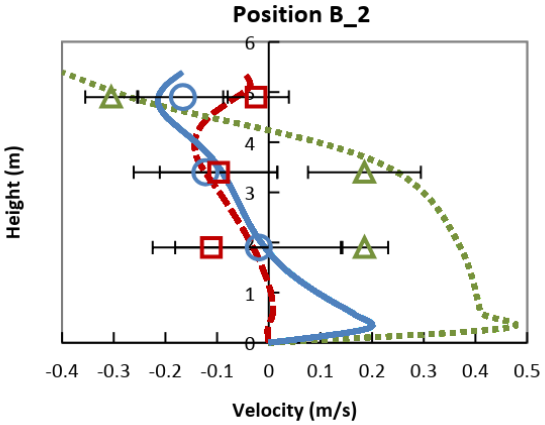

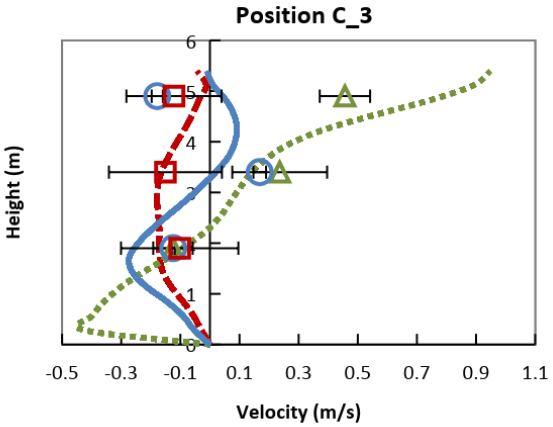

Figure 8. Comparison of fluid velocity components calculated and measured with air.

3.2.4 Two-phase-flow performance using PBM

[+] schiva@uji.es, Universitat Jaume I, Mechanical Engineering and Construction Department. Av. Vicent Sos Baynat, s/n 12071 Castellón (Spain). Telf: +34 964 728 141

The main region of interest to be studied in the two-phase flow is the zone over the grids where the hydrodynamics is especially complex. Figure 9 shows the gas hold-up plotted at the plane d-d' defined in figure 8 knowing this contour is well representative of the gas performance. The motion of the bubble columns induces a vertical convective flux cell before and after the grids of the diffusers, represented throughout equally spaced vectors. This is the reason the horizontal mixed liquor velocity decreases inside the outer channel. The three main plumes of air bubbles, corresponding to the three diffusers grids, showed good stability for the steady state calculation. Once achieved a certain height, they merged into one due to the layout of the grids which maintain them close enough to produce this phenomenon. Moreover, the free surface approach used, allowed the increase of the mixed liquor level to be analysed. This contributed to induce the convective flux cell: a backflow in the first half region over the grids, and an increase of the flux velocity in the second half part alongside the free surface. Figure 9 shows also the vortex core regions displaying the turbulent structures over the mixed liquor beyond the grid region.

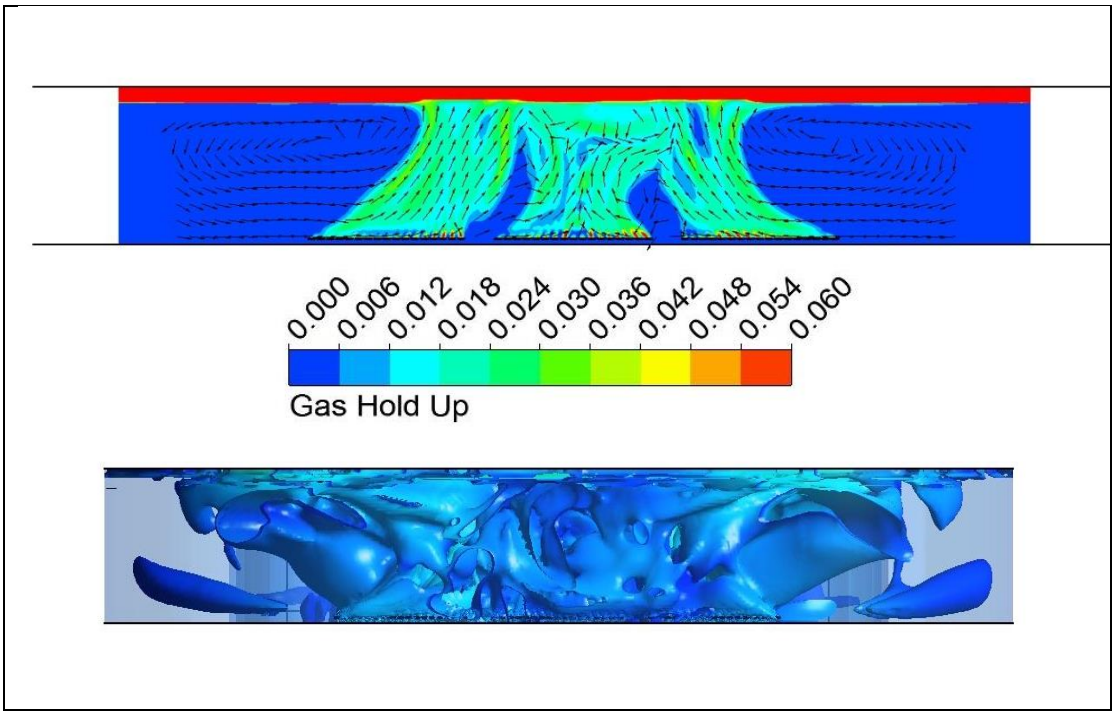

+ schiva@uji.es, Universitat Jaume I, Mechanical Engineering and Construction Department. Av. Vicent Sos Baynat, s/n 12071 Castellón (Spain). Telf: +34 964 728 141

Figure 9. Contour of gas hold-up air bubble plumes (above) and the vortex core regions in 3D (below) both plotted in section d-d' (figure 8).

To analyse the results from the PBM, one must distinguish between the hold-up provided by the dispersed phase, $\alpha_{\square}$,and the i-th group hold-up provided, $\alpha_{\square}$, defined as $\alpha_{\square}=\square_{\square}\square_{\square}$, being the size fraction of the i-th group. As the sum of the size fractions for all the groups must sum unity, the sum of the group hold-ups must equal the hold-up.

We start the analysis by isolating the volume in the domain where the hold-up exceeds 0.05% for all of the groups (Fig. 10). The histogram in figure 10 shows the diameter distribution of the bubbles in this region. The effects of bubble coalescence can be clearly noticed given that diameters lower than 3 mm (size of the injected bubbles) can be neglected. Also, note that bubbles with diameters between 3 and 4mm represented 75% of the volume while bubble diameters greater than 4 mm occupied about 25% of the volume. The highest diameter calculated corresponded to 7.46mm. From this histogram, one can finally conclude that bubble break-up is negligible.

Figure 11 shows the volume where there is presence of large bubbles represented by Groups 7 to 10. These regions are located mainly in the sides of the channel. This is caused by the increased turbulence in the limits of the bubble plume close to the walls. The bubble plume raises the liquid, whereas the non-slip condition at the wall prevents its movement. The resulting high-shear and turbulence level enhances the bubble collisions, thus increasing the bubble coalescence. Moreover, it was determined that the coalescence in these regions is so high due to there are no bubbles with diameters below 4 mm.

[+] schiva@uji.es, Universitat Jaume I, Mechanical Engineering and Construction Department. Av. Vicent Sos Baynat, s/n 12071 Castellón (Spain). Telf: +34 964 728 141

To get a better insight into the break-up, a third volume was selected corresponding to regions where there is presence of the Groups 1 and 2 (Fig. 12). Again, these regions are located near the walls, as the main mechanism for the bubble break-up consists of the shearing-off of large bubbles. Only 1% of this volume is occupied by bubbles smaller than 3 mm. This result can be interpreted given the shearing-off mechanism that produces the small bubbles. Big bubbles are sheared by high velocity gradients near the wall and rarely split into two equal volume smaller bubbles [44], but rather into one big and one small bubble.

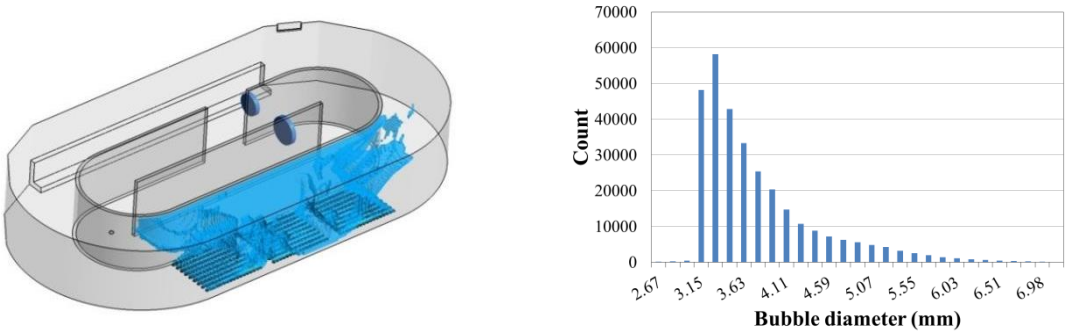

Figure 10. Isovolume of all the groups of bubbles (left) and its bubble size distribution (right)

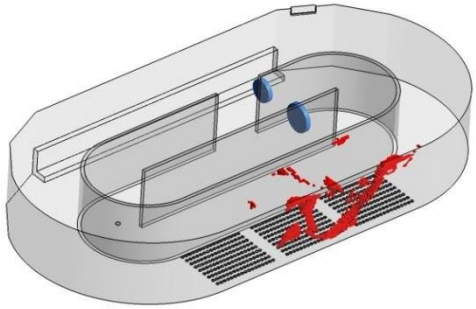

Figure 11. Isovolume of bubbles of groups 7 to 10

+ schiva@uji.es, Universitat Jaume I, Mechanical Engineering and Construction Department. Av. Vicent Sos Baynat, s/n 12071 Castellón (Spain). Telf: +34 964 728 141

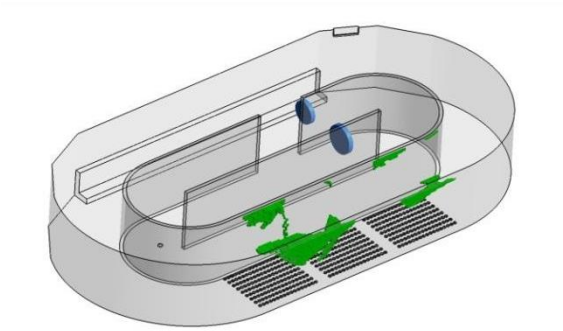

Figure 12. Isovolume of bubbles of groups 1 and 2

Figure 13 represents the interfacial area density calculated by the PBM inside a volume of air. This was defined by selecting the hold-up below to 3.5% in order to exclude the free-surface contribution. The two highest bars of the histogram were concentrated around 15 m^{-1}. Values between 30 and 60 m^{-1} represented an important contribution of 42% of the volume, while values under 10 m^{-1} and above 60 m^{-1} represented about 7% in each case.

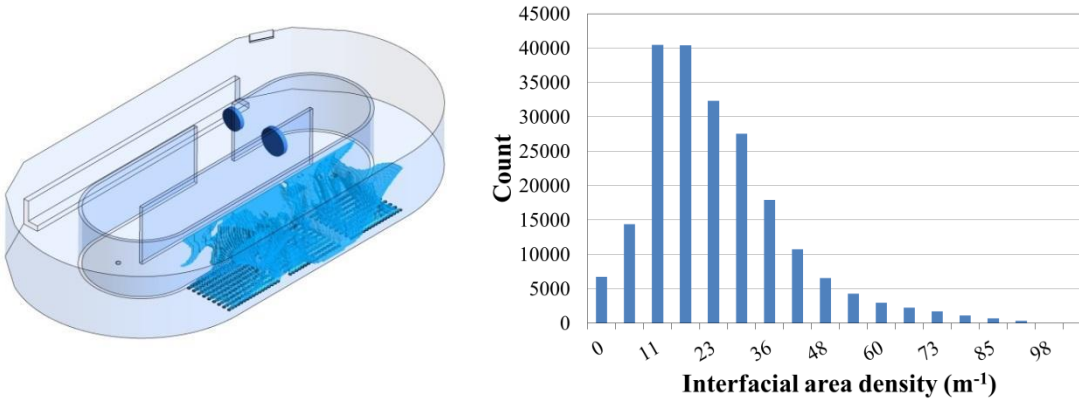

Figure 13. Isovolume of hold-up represented up to 3.5% (left), and its corresponding interfacial area density (right)

Figure 14 shows the plumes across the width of the channel by means of the hold-up, section e-e' (indicated in Fig. 9). It can be considered a representative performance of the dispersed phase. Note that the air bubbles are injected through the diffusers

+ schiva@uji.es, Universitat Jaume I, Mechanical Engineering and Construction Department. Av. Vicent Sos Baynat, s/n 12071 Castellón (Spain). Telf: +34 964 728 141

vertically, but every column gets attracted by the one that is placed next to it towards the interior of the channel. Consequently, bubble columns tend to group/collide (see figure 9 for a similar effect). Also, near to the walls recirculation vortexes do appear. In this case, the asymmetry of the diffuser distribution along the width of the tank enhances this effect, which is especially noticeable over the recirculation formed in the bottom left corner. Figure 16 shows also the mean bubble diameter distribution. Note that the larger bubbles tend to go near the walls. This is caused by two phenomena: first, the lift tends to direct them towards the walls; second, bubble coalescence is driven by turbulent collisions, matching the regions with higher turbulence levels with higher bubble diameters. Also, turbulent impact of eddies against big bubbles can lead to breakup, which can lead to regions with smaller diameters near regions with large bubbles and turbulence, as for example near the air-liquid interface. In addition, ascending bubbles act as a source of turbulence, so the turbulence level increases with the height over the channel ground. Hence, a certain trend can be observed where the larger bubbles take place at the upper region and close to the walls, while the medium sizes are located at the central and the bottom zone.

[+] schiva@uji.es, Universitat Jaume I, Mechanical Engineering and Construction Department. Av. Vicent Sos Baynat, s/n 12071 Castellón (Spain). Telf: +34 964 728 141

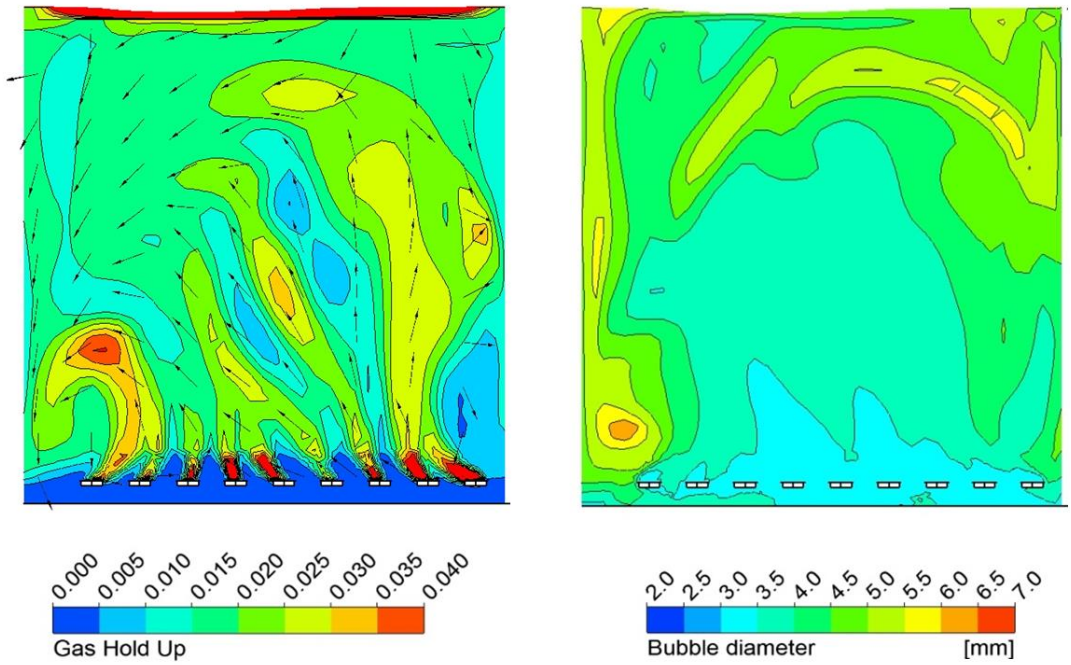

Figure 14. Hold-up (left) and bubble diameter (right) both in section e-e'

Multiphase modelling is needed when the purpose of the CFD model aims for a deeper knowledge of the dispersed phase; it entails certain complexity level, and difficulties of validating the submodels, as well as limitations in computational power. To sum up, the multiphase modelling depicts a scenario where the bubble plumes generated by the diffusers collide leading to coalescence. This is anundesired effect, as the aeration efficiency is reduced. Given the difficulties to measure the actual sizes of the bubbles in real tanks, CFD simulations can be used as a tool for the optimization of the air flow injected through the diffusers, taking into account the influence of both increase in turbulence and bubble sizes onto the mass transfer. Also, the multiphase simulation shows that a bubble column filling the width of the channel significantly reduces the flow speed in the whole tank, as it generates a drag that tends to stop the flow. This might be considered a faulty hydrodynamic design, and might be of interest for future studies.

[+] schiva@uji.es, Universitat Jaume I, Mechanical Engineering and Construction Department. Av. Vicent Sos Baynat, s/n 12071 Castellón (Spain). Telf: +34 964 728 141

3.3 Optimization

The positioning of the propellers within the tank is based on various heuristic guidelines and correlations, for instance, increasing the surface turbulence facilitates the entrainment of oxygen, not desirable for anoxic tanks, and the correct vertical position can ensure the suspension of the solids minimizing the wall friction [45].

The set of the CFD models of this section, study alternatives to the initial configuration, taking into account the standard regulation specified by different manufacturers [45, 46] provided that the minimum distance to the walls is guaranteed.

Several configurations were tested modifying the position of the two propellers for minimizing the incoming flow through the channel spacing, which affected negatively the hydrodynamic behaviour in the inner channel. Considering that an improvement in the fluid behaviour within the tank will provide a better performance of the AS process, it has been taken into account alternative configurations for the propellers layout to enhance hydrodynamics and therefore, the biological nutrient removal process.

Figure 15 shows the results of the calculations of the 6 configurations simulated. They were analysed considering these two requirements: (1) minimizing the incoming flux entering from the outer to the inner channel and (2) the accomplishment of the distance to the wall. As a result, a modified configuration was proposed. Firstly, a detailed study of fluid flow was performed in the channel spacing (refer to supplementary material). This zone was considered one of the most critical because of the coexistence of both the incoming and the outcoming flow. Based on the criteria explained above, the configuration 2 was selected as the optimal proposal which

[+] schiva@uji.es, Universitat Jaume I, Mechanical Engineering and Construction Department. Av. Vicent Sos Baynat, s/n 12071 Castellón (Spain). Telf: +34 964 728 141

minimized the mass flow entering from the outer to the inner channel drastically, improving the fluid behaviour inside the inner channel (figure 16).

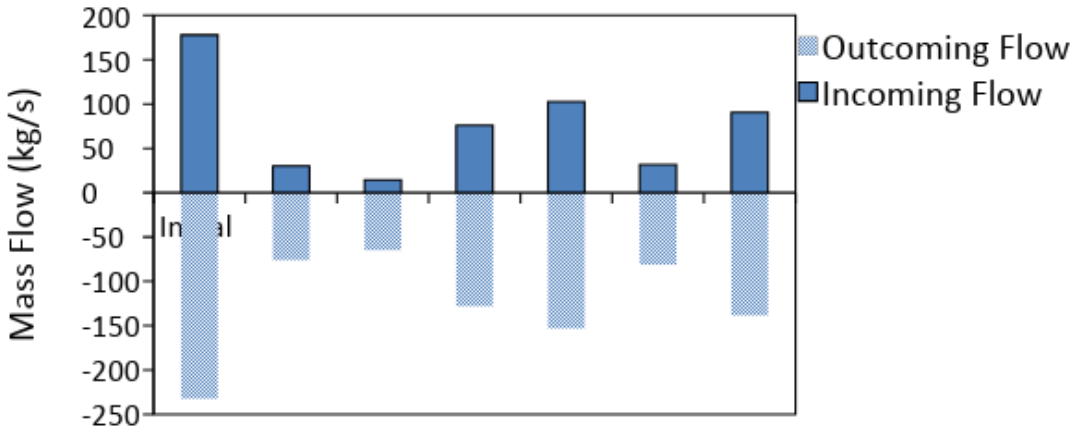

Figure 15. Mass flow rate incoming and outcoming through the channel spacing

Figures 16 and 17 show the optimal configuration selected which improves the mixing in the inner channel, reducing the low velocity zones and minimizes the entrainment of the fluid flow from the outer to the inner channel by 92%. This configuration maintained the average fluid velocity along the outer channel increasing the average fluid velocity in the inner channel due to the internal propeller, and inducing a more stable plume of fluid.

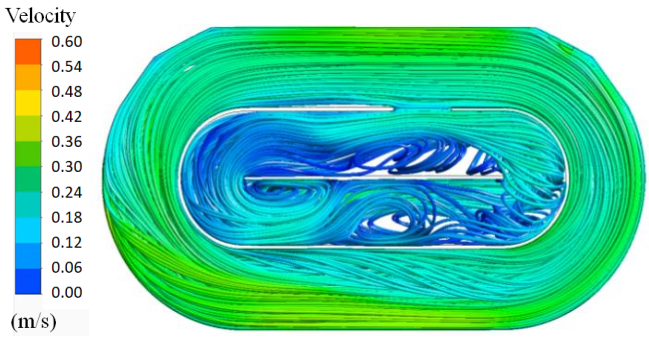

Figure 16. Velocity of the streamlines at the optimum configuration

+ schiva@uji.es, Universitat Jaume I, Mechanical Engineering and Construction Department. Av. Vicent Sos Baynat, s/n 12071 Castellón (Spain). Telf: +34 964 728 141

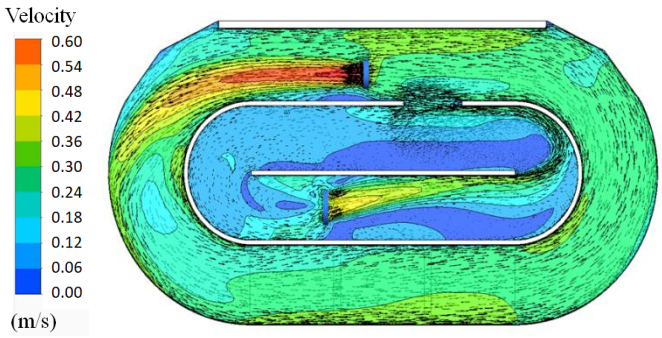

Figure 17. Velocity contour at 2m high

Detailed information about the configurations tested and the results of the optimization study by CFD simulation as well as the manufacturer's recommendations for the location of the propellers have been included as supplementary material.

4. Conclusions

A two-phase CFD model including a PBM was performed to reproduce the interaction between the dispersed phase motion and the liquid behaviour inside the aeration tank. Despite the high computing time and limitations of PBM validation, it is important to highlight that this is valuable when it is necessary to study carefully the design diffuser layouts in the oxidation ditch. The main results from this study are:

- Tracer tests can provide the global fluid behaviour of each channel when there is a clear separation between them. Inadequate mixing was determined for the inner channel by the RTD obtained at the channel spacing.
- A hydrodynamic analysis was performed with and without air. It was extensively validated by means of the 3 velocity component measurements.

[+] schiva@uji.es, Universitat Jaume I, Mechanical Engineering and Construction Department. Av. Vicent Sos Baynat, s/n 12071 Castellón (Spain). Telf: +34 964 728 141

- Single-phase model approach provided good results when there was no dispersed phase. Defects of the fluid behaviour were detected and calculated successfully in steady state.
- The two-phase flow CFD model investigated showed a good stability of the bubble plumes. The free-surface approach allowed the backflow measured experimentally at the interface to be calculated.
- The multiphase CFD model predicted a reduction of the fluid velocity in the outer channel by 60% with respect to the non aerated case. This prediction was in good agreement with experimental measurements.

- The analysis of the bubble size and the interfacial area density revealed that, in the oxidation ditch performance, the coalescence is predominant, and the break-up can be neglected.
- The best mixing option to reduce the entrainment of the fluid flow from the outer to the inner channel was successfully investigated by the CFD model under a variety of operational conditions depending on the location of the propellers. The optimal configuration provided a reduction of 92%.

Acknowledgements

The authors would like to gratefully acknowledge the economic and technical support provided by CADAGUA, the technical support provided by Entidad de Saneamiento y Depuración de la Región de Murcia (ESAMUR) and the project 16I367 from Universitat Jaume I.

[+] schiva@uji.es, Universitat Jaume I, Mechanical Engineering and Construction Department. Av. Vicent Sos Baynat, s/n 12071 Castellón (Spain). Telf: +34 964 728 141

References

[1] M. Gresch, D. Braun, W. Gujer, Using reactive tracers to detect flow field anomalies in water treatment reactors, Water Res. 45 (2010) 1984–1994.

[2] A.M. Karpinska, J. Bridgeman, CFD-aided modelling of activated sludge systems e A critical review Standard Method of Moments, Water Res. 88 (2016) 861–879.

[3] G.C. Glover, C. Printemps, K. Essemiani, J. Meinhold, Modelling of wastewater treatment plants - How far shall we go with sophisticated modelling tools?, Water Sci. Technol. 53 (2006) 79–89.

[4] Metcalf & Eddy, Wastewater Engineering: Treatment and Reuse, 4th Editio, McGraw-Hill, 2004.

[5] M. Gresch, M. Armbruster, D. Braun, W. Gujer, Effects of aeration patterns on the flow field in wastewater aeration tanks, Water Res. 45 (2010) 810–818.

[6] R. Hreiz, O. Potier, J. Wicks, J.-M. Commenge, CFD Investigation of the effects of bubble aerator layouts on hydrodynamics of an activated sludge channel reactor, Environ. Technol. 0 (2018) 1–14.

[7] Cockx, Z. Do-Quang, J.. Audic, a Liné, M. Roustan, Global and local mass transfer coefficients in waste water treatment process by computational fluid dynamics, Chem. Eng. Process. Process Intensif. 40 (2001) 187–194.

[8a] Y. Fayolle, S. Gillot, M. Roustan, A. Héduit, Oxygen transfer prediction in aeration tanks using CFD. Chemical Engineering Science 62 (2007) 7163–7171.

[8b] Y. Fayolle, S. Gillot, A. Cockx, L. Bensinhom, M. Roustan, A. Héduit, *In situ* characterisation of local hydrodynamic parameters in closed-loop aeration tanks. Chemical Engineering Journal 158 (2010) 207–212.

[9] J. Laurent, R.W. Samstag, J.M. Ducoste, A. Griborio, I. Nopens, D.J. Batstone, J.D. Wicks, S. Saunders, O. Potier, A protocol for the use of computational fluid dynamics as a supportive tool for wastewater treatment plant modelling, Water Sci. Technol. 70 (2014) 1575–1584.

[10] N. Eshtiaghi, F. Markis, S.D. Yap, J.C. Baudez, P. Slatter, Rheological characterisation of municipal sludge: A review, Water Res. 47 (2013).

[11] M. Brannock, Y. Wang, G. Leslie, Mixing characterisation of full-scale membrane bioreactors: CFD modelling with experimental validation, Water Res. 44 (2010) 3181–3191.

[12] H. Xie, J. Yang, Y. Hu, H. Zhang, Y. Yang, K. Zhang, Simulation of flow field and sludge settling in a full-scale oxidation ditch by using a two-phase flow CFD model, 109 (2014) 296–305.

[+] schiva@uji.es, Universitat Jaume I, Mechanical Engineering and Construction Department. Av. Vicent Sos Baynat, s/n 12071 Castellón (Spain). Telf: +34 964 728 141

[13] J. Aubin, D.F. Fletcherb, C. Xuereba, 2004. Modeling turbulent flow in stirred tanks with CFD: the influence of the modelling approach, turbulence model and numerical scheme. Experimental Thermal and Fluid Science, 28, 5, 431-445

[14] Y. Le Moullec, O. Potier, C. Gentric, J.P. Leclerc, Activated sludge pilot plant : Comparison between experimental and predicted concentration profiles using three different modelling approaches, 5 (2011).

[15] R.W. Samstag, J.J. Ducoste, A. Griborio, I. Nopens, D.J. Batstone, J.D. Wicks, S. Saunders, E.A. Wicklein, G. Kenny, J. Laurent, CFD for wastewater treatment: An overview, Water Sci. Technol. 74 (2016).

[16] Nopens, I., Torfs, E., Ducoste, J., Vanrolleghem, P., and Gernaey, K. (2014). Population Balance Models: A useful complementary modelling framework for future WWTP modelling. In Proceedings. 4th IWA/WEF Wastewater treatment modelling seminar (pp. 129-138). Water Environment Federation.

[17] Wang, T. (2011). Simulation of bubble column reactors using CFD coupled with a population balance model, Chem. Sci. Eng., 5, 162-172.

[18] Marchisio, DL., Fox, RO. Solution of population balance equation using the direct quadrature method of moments. Journal of aerosol Science, 36, 1, 43-73, (2005)

[19] R.W. Samstag, E.A. Wicklein, R.D. Reardon, R.J. Leetch, R.M. Parks, C.D. Groff, C. Engineers, W. Park, Field and CFD Analysis of Jet Aeration and Mixing, Proc. WEFTEC Conf. (2012). doi:10.2175/193864712811708301.

[20] Y. Le Moullec, O. Potier, C. Gentric, J. Pierre Leclerc, Flow field and residence time distribution simulation of a cross-flow gas-liquid wastewater treatment reactor using CFD, Chem. Eng. Sci. 63 (2008) 2436–2449.

[21] O. Potier, J.P. Leclerc, M.N. Pons, Influence of geometrical and operational parameters on the axial dispersion in an aereated channel reactor, Water Res. 39 (2005) 4454–4462.

[22] E. Wicklein, D.J. Batstone, J. Ducoste, J. Laurent, A. Griborio, J. Wicks, S. Saunders, R. Samstag, O. Potier, I. Nopens, Good modelling practice in applying computational fluid dynamics for WWTP modelling, Water Sci. Technol. 73 (2016).

[23] J. Climent, L. Basiero, J.G. Berlanga, S. Chiva, Biological reactor retrofitting using CFD-ASM modelling, 348 (2018) 1–14.

[24] F.R. Menter, Two-Equation Eddy-Viscosity Turbulence Models for Engineering Applications, AIAA J. 32 (1994) 1598–1605.

[25] ANSYS® Academic Research, Release 16.2, Help System, ANSYS CFX

+ schiva@uji.es, Universitat Jaume I, Mechanical Engineering and Construction Department. Av. Vicent Sos Baynat, s/n 12071 Castellón (Spain). Telf: +34 964 728 141

Reference Guide, ANSYS Inc, n.d.

[26] U. Rehman, Next generation bioreactor models for wastewater treatment systems by means of detailed combined modelling of mixing and biokinetics, 2016. http://hdl.handle.net/1854/LU-8109100.

[27] S. Lo, "Application of the MUSIG model to bubbly flows", AEA Technology, 1996, AEAT-1096.

[28] H. Luo, H.F Svendsen, Theoretical model for drop and bubble breakup in turbulent dispersions (1996). A.I.Ch.E. J. 42, 1225–1233.

[29] M. J. Prince, H.W. Blanch, "Bubble coalescence and break-up in air-sparged bubble columns", AIChE J., 36, 1990, pp. 1485–1499.

[30] Wu, Q., et al., 1998. One-group interfacial area transport in vertical bubbly flow. International Journal of Heat and Mass Transfer 41, 1103–1112.

[31a] Wang, T.F., et al., 2005a. Theoretical prediction of flow regime transition in bubble columns by the population balance model. Chemical Engineering Science 60, 6199–6209.

[31b] Wang, T.F., et al., 2005b. Population balance model for gas–liquid flows: Influence of bubble coalescence and breakup models. Industrial and Engineering Chemistry Research 44, 7540–7549.

[32] M. Jamialahmadi, C. Branch, H. Müller-Steinhagen. Terminal bubble rise velocity in liquids. Trans. Inst. Chem. Eng., 72 (1994), pp. 119-122

[33] J.U, Brackbill, D.B., Kothe, and C.Zemach, "A Continuum Method for Modelling Surface Tension", Journal of Computational Physics 100:335-354, 1992.

[34] Ishii, M., and N. Zuber, 1979, Drag coefficient and relative velocity in bubbly, droplet or particulate flows, AIChE J. 25, 843-855

[35] Favre Averaged Drag Model Burns, A.D.B., Frank, Th., Hamill, I., and Shi, J-M., "The Favre Averaged Drag Model for Turbulent Dispersion in Eulerian Multi-Phase Flows", 5th International Conference on Multiphase Flow, ICMF-2004, Yokohama, Japan.

[36] SATO, Y. and SEKOGUCHI, K., (1975), "Liquid velocity distribution in two-phase bybbly flow", Int. J. Multiphase Flow, 2, 79.

[37] Rzehak, R, Krepper, E., Liao, Y., Ziegenhein, Th., Kriebitzsch, S. and Lucas, D. (2015). Baseline model for the simulation of bubbly flows. Chemical Engineering Science 38, 1972-1978

[38] The Legendre and Magnaudet Lift Force Model Legendre, D. and Magnaudet, J., "The lift force on a spherical bubble in a viscous linear shear flow", J. Fluid

[+] schiva@uji.es, Universitat Jaume I, Mechanical Engineering and Construction Department. Av. Vicent Sos Baynat, s/n 12071 Castellón (Spain). Telf: +34 964 728 141

Mech., 368, pp. 81–126, 1998

[39] O. Levenspiel, Chemical Engineering Reactor, John Wiey, New York, 1972.

[40] L. Rieger, S. Gillot, G. Langergraber, T. Ohtsuki, A. Shaw, I. Takács, S. Winkler, Guidelines for Using Activated Sludge Models, IWA Publishing, London, 2013.

[41] Improvement of Acoustic Doppler Velocimetry in bubbly flow measurements as applied to river characterization for kinetic turbines International Journal of Multiphase Flow, Volume 37, Issue 8, October 2011, Pages 919-929 Amir Hossein Birjandi, Eric Louis Bibeau

[42] L.J. Burrows, A.J. Stokes, J.R. West, C.F. Forster, A.D. Martin, Evaluation of different analytical methods for tracer studies in aeration lanes of activated sludge plants, Water Res. 33 (1999) 367–374.

[43] Derek York, 1966. ‘‘Least-squares fitting of a straight line,’’ Can. J. Phys. 44, 1079–1086

[44] J.C. Lasheras, C. Eastwood, C. Martínez-Bazán, amd J.L.Montañés, 2002.A review of statistical models for the break-up of an immiscible fluid immersed into a fully developed turbulent flow. International Journal of Multiphase Flow 28, 247-278.

[45] Agitadores sumergibles FLYGT (2013). Conceptos básicos de cálculo.

[46] Agitadores sumergibles WILO (2014). Jornada WILO-SDM.

[+] schiva@uji.es, Universitat Jaume I, Mechanical Engineering and Construction Department. Av. Vicent Sos Baynat, s/n 12071 Castellón (Spain). Telf: +34 964 728 141